

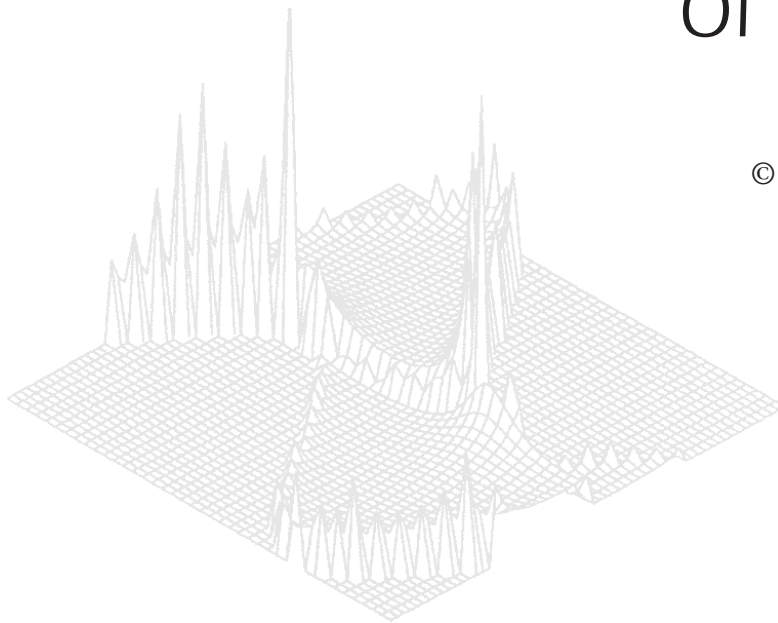
---

**C S I R O   P U B L I S H I N G**

---

# Australian Journal of Physics

Volume 50, 1997  
© CSIRO Australia 1997



A journal for the publication of  
original research in all branches of physics

**[www.publish.csiro.au/journals/ajp](http://www.publish.csiro.au/journals/ajp)**

All enquiries and manuscripts should be directed to

*Australian Journal of Physics*

**CSIRO PUBLISHING**

PO Box 1139 (150 Oxford St)

Collingwood

Vic. 3066

Australia

Telephone: 61 3 9662 7626

Facsimile: 61 3 9662 7611

Email: [peter.robertson@publish.csiro.au](mailto:peter.robertson@publish.csiro.au)



Published by **CSIRO PUBLISHING**  
for CSIRO Australia and  
the Australian Academy of Science



## Modeling of a Micro-streamer Initiation and Development of ArF Excimer Laser Discharges\*

*H. Akashi*<sup>A</sup>, *Y. Sakai*<sup>B</sup> and *H. Tagashira*<sup>C</sup>

<sup>A</sup> Department of Applied Physics, National Defense Academy, Yokosuka 239, Japan.

<sup>B</sup> Department of Electrical Engineering, Hokkaido University, Sapporo 060, Japan.

<sup>C</sup> Department of Electrical Engineering, Hokkaido Institute of Technology, Sapporo 006, Japan.

### *Abstract*

The dynamics of a constricted filamentary or ‘micro-streamer’ discharge in a discharge-excited ArF excimer laser has been examined using a two-dimensional fluid model. The entire process on a micro-streamer, from its initiation and development to extinction, is shown. In the present model, a micro-streamer is triggered at protrusions which always exist on cathode surfaces, and develops in the direction of the anode assisted by the high field induced by space charge. A rise in the gas temperature in the micro-streamer in the vicinity of a cathode is seen, and which is found to play an important role in its development. The effect of preionisation electron density  $n_{e0}$  on the streamer development is also examined, and the streamer is found to extend significantly when  $n_{e0}$  becomes low. The results are explained in connection with experimental observations.

### 1. Introduction

Discharge-excited excimer lasers have been developed to utilise in processing VLSI and other devices, as an UV light source. In order to make their intensity, efficiency and repetition rate higher, and their gas lifetime longer, one of the key technologies is to sustain arc-free large volume, high energy density glow discharges. Accordingly, first of all, we have to make clear the reason why a filamentary discharge or ‘micro-streamer’ which might grow into an arc discharge occurs in a volume discharge and the process of how it develops. After that we may find a way how to suppress the micro-streamer and arc. Generally, filamentary discharges have been reported to occur because of halogen donor depression, non-uniformity of the preionisation electron-ion pairs density, etc. (Taylor 1986; Kushner 1991). However, the mechanism of its generation and development into a micro-arc in atmospheric pressure excimer laser discharges is not well understood.

Recently the dynamic behaviour of micro-discharges in XeCl excimer laser discharges has been observed optically by Makarov (1995), Makarov and Bychkov (1996) and Dreiskemper and Boetticher (1995). In their works the micro-discharges were shown to occur in the cathode fall region and develop in the direction of the anode. On the other hand, one-dimensional modeling for an ArF laser

\* Dedicated to Professor Robert W. Crompton on the occasion of his seventieth birthday.

discharge, taking account of the space charge effect, has suggested the possibility of generation of a discharge instability in the vicinity of the cathode because the space charge distortion becomes extremely high (Akashi *et al.* 1994, 1995).

In this paper, using a two-dimensional fluid model in which the local electric field distortion and gas temperature are properly considered, we investigate the generation and spatio-temporal evolution of a constricted micro-streamer in a discharge-excited ArF excimer laser medium. It is assumed that a filamentary discharge is initiated first by field emission of electrons at a sharp protrusion on a cathode surface. After that, the development of the micro-streamer is studied self-consistently. The results are compared phenomenologically with dynamic features of experimental observations (Makarov 1995; Makarov and Bychkov 1996; Dreiskemper and Boettcher 1995).

## 2. Modeling

### (2a) Basic Equations

Using the electron kinetic data in a plasma obtained by a Boltzmann equation analysis for a gas mixture of Ar, F<sub>2</sub> and He, the following equations are incorporated; the continuity equations for electrons, positive ions for Ar and He and negative ions for F<sub>2</sub>, the equations for photo-electron emission from the cathode and for electron energy conservation, the rate equations for formation of ArF\* and excited species, and Poisson's equation (Akashi *et al.* 1994, 1995).

As a coaxial symmetry of the discharge space is assumed, the number densities  $n_j$  for the  $j$ th species of particles (electrons, Ar<sup>+</sup>, He<sup>+</sup>, F<sup>-</sup> and excited particles) are functions of two coordinates  $z(x, r)$ , where  $x$  is the distance from the cathode in the direction of  $-E$  (the external field), and  $r$  the radial direction from the protrusion (see Fig. 3 below), at time  $t$ . They are written as

$$\begin{aligned} \frac{\partial n_j}{\partial t} + \frac{\partial}{\partial x} \Gamma_{jx} + \frac{1}{r} \frac{\partial}{\partial r} (r \Gamma_{jr}) &= k_{i,j} n_j N, \\ \Gamma_{jx} &= -\mu_{jx} n_j - D_{jx} \frac{\partial}{\partial x} n_j, \\ \Gamma_{jr} &= -\mu_{jr} n_j - D_{jr} \frac{\partial}{\partial r} n_j, \end{aligned} \quad (1)$$

where  $k_{i,j}$  indicates the  $i$ th reaction rate coefficient for the  $j$ th species. Here  $\mu_j$  and  $D_j$  are the mobility and diffusion coefficient for the  $j$ th species, respectively, and  $N$  is the gas number density.

The mean electron energy  $\bar{\varepsilon}(z, t)$  is obtained using the following energy conservation equation, assuming the electron energy distribution is Maxwellian (Graves and Jensen 1986):

$$\begin{aligned} \frac{\partial}{\partial t} (n_e \bar{\varepsilon}) + \frac{\partial}{\partial x} \left( \frac{5}{3} \bar{\varepsilon} \Gamma_{ex} + q_x \right) + \frac{1}{r} \frac{\partial}{\partial r} \left\{ r \left( \frac{5}{3} \bar{\varepsilon} \Gamma_{er} + q_r \right) \right\} &= e \Gamma_{ex} E_x + e \Gamma_{er} E_r \\ &\quad - k_{i,j} n_e N H_i - k_{i,j} n_e N H_{ex,j} - k_a n_e N \bar{\varepsilon}, \\ q &= -\frac{2}{3} \kappa \nabla \bar{\varepsilon}, \quad \kappa = \frac{5}{2} n_e D_e, \end{aligned} \quad (2)$$

where  $H_i$ ,  $H_{ex}$  and  $\kappa$  are the ionisation and excitation potentials, and the electron thermal conductivity, respectively.

The time dependent local field  $E(z, t)$  is given using Poisson's equation as

$$\frac{\partial^2 V}{\partial x^2} + \frac{1}{r} \frac{\partial V}{\partial r} + \frac{\partial^2 V}{\partial r^2} = -\frac{e}{\varepsilon_0} \rho, \quad (3)$$

and at  $r = 0$

$$\frac{\partial^2 V}{\partial x^2} + 2 \frac{\partial^2 V}{\partial r^2} = -\frac{e}{\varepsilon_0} \rho,$$

with

$$E = -\text{grad}V, \quad \rho = n_{Ar^+} + n_{He^+} - n_{F^-} - n_e.$$

Here,  $e$  and  $\varepsilon_0$  are the charge of an electron and the permittivity in vacuo respectively.

The gas temperature  $T_g$  is determined by the following energy conservation equation for neutral particles:

$$\begin{aligned} \frac{5}{2} k N \frac{\partial T_g}{\partial t} &= \frac{\partial}{\partial x} \Gamma_{g_x} + \frac{1}{r} \frac{\partial}{\partial r} r \Gamma_{g_r} + n_e e \mu_e E^2, \\ \Gamma_g &= \kappa \nabla T_g, \end{aligned} \quad (4)$$

where  $k$  and  $\kappa_g$  are the Boltzmann constant and the gas thermal conductivity. In this calculation, the gas pressure is assumed to be uniform all over the discharge space.

Only the secondary emission of electrons by photons from the cathode is considered, since the time scale of this discharge is short ( $\sim 100$  ns). The photo-electron number density  $n_{ep}(z_c, t)$ ,  $z_c = (0, r)$ , at the cathode is given by the following equation (Morrow 1985):

$$\begin{aligned} n_{ep}(z_c, t) &= \frac{1}{W_v(z_c, t)} \frac{\gamma_p}{\tau} \int_0^t \exp\left(\frac{-t-t'}{\tau}\right) \\ &\times \int_{-r}^r \int_0^d n_e(z, t') N k_{ex,j} \Omega(z) \exp(-\mu z) dz dt', \end{aligned} \quad (5)$$

where  $W_v(z_c, t)$ ,  $\gamma_p$ ,  $\tau$ ,  $\Omega(z)$  and  $\mu$  are the drift velocity of photoelectrons, the efficiency factor for a photon to release photoelectrons from the cathode, the lifetime of the radiative excited states of the gas atoms, the solid angle at the cathode subtended by a disk of the charge at  $x$ , and the photon absorption coefficient in the gas, respectively. Further,  $k_{ex,j}$  is the excitation rate coefficient for  $j$ th type molecules.

Boundary conditions at the cathode ( $x = 0$ ) for equations (1)–(4) are taken as in a previous paper (Akashi *et al.* 1994) except for the sharp protrusion on the cathode. At the protrusion field emission of electrons is assumed due to a strong local field. At the cathode ( $z_c = (0, r)$ ), the  $n_e$ ,  $n_+$  and  $n_-$  and the potential  $V$

and temperature for electrons  $T_e$  and gas  $T_g$  are taken, respectively, as

$$\begin{aligned} n_e(z_c, t) &= n_{ep}(z_c, t), & n_+(z_c, t) &= \frac{\Gamma_+(\Delta z_c, t)}{W_+(z_c, t)}, \\ n_-(z_c, t) &= 0, & V(z_c, t) &= 0, \\ T_e(z_c, t) &= 0.5 \text{ eV}, & T_g(z_c, t) &= 273 \cdot 15 \text{ K}. \end{aligned}$$

At the anode ( $z_a = (d, r)$ ), they are

$$\begin{aligned} n_e(z_a, t) &= n_+(z_a, t) = n_-(z_a, t) = 0, \\ V(z_a, t) &= V_g, \\ T_g(z_a, t) &= 273 \cdot 15 \text{ K}, \end{aligned}$$

where  $V_g$  is the discharge voltage. In the radial direction, at  $z_r = (x, r_{\max} = 0.5 \text{ cm})$ , the following conditions are assumed,

$$\begin{aligned} \frac{\partial n_j(z_r, t)}{\partial r} &= 0, & \frac{\partial V(z_r, t)}{\partial r} &= 0, \\ \frac{\partial T_e(z_r, t)}{\partial r} &= 0, & \frac{\partial T_g(z_r, t)}{\partial r} &= 0. \end{aligned}$$

For the second shot of discharge, the distribution of gas temperatures near the protrusion is taken (see Fig. 5c below), assuming that the distribution obtained by the first shot is kept to the following shot.

### (2b) Excitation Circuit

A typical charge-transfer circuit is adopted as an equivalent excitation circuit for excimer lasers, as shown in Fig. 1, which taken from a previous paper (Akashi *et al.* 1994). The equivalent resistance of the discharge is given as  $R_D = V_g/I_g$ . The discharge current  $I_g$  is written as

$$I_g(t) = \frac{e}{d} \int_0^d dx \int 2\pi r (W_+ n_+ - W_r n_e - W_- n_-) dr. \quad (6)$$

The voltage  $V_g$  is given by solving the circuit equations for Fig. 1 in the same way as shown in Akashi *et al.* (1994).

### (2c) Swarm Parameters for Electrons and Ions

The reaction rate coefficients for electrons and neutral excited particles considered in this work are the same as those taken by Akashi *et al.* (1994). The values of  $k_{i,e}$  and diffusion coefficient for electrons are given by a Boltzmann equation analysis as functions of the mean electron energy  $\bar{\epsilon}$ , and for the drift velocity

and the diffusion coefficients for electrons and ions, a local field approximation is taken.

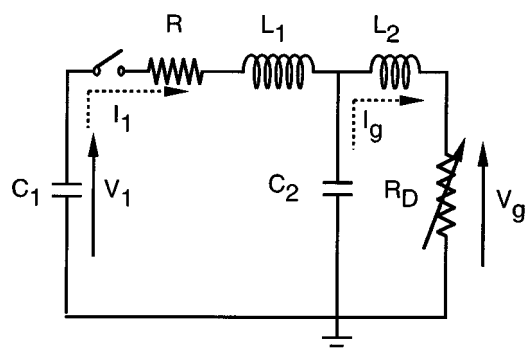


**Fig. 1.** Excitation circuit of a self-sustained discharge ArF laser:  $R_D$  is the effective resistance of the discharge plasma,  $C_1 = 10$  nF,  $C_2 = 1.5$  nF,  $R = 0.1\Omega$ ,  $L_1 = 100$  nH,  $L_2 = 20$  nH, and  $V_1 = 20$  kV at  $t = 0$ . The discharge volume is  $1\text{ cm} \times 90\text{ cm}^2$  (gap distance  $d$  times the discharge cross section  $S$ ).

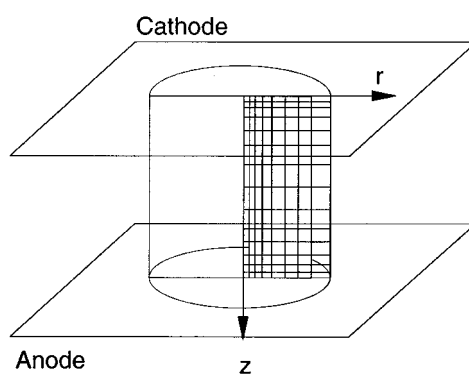


**Fig. 2.** Mesh configuration of the discharge space for numerical calculation.

#### (2d) Numerical Method and Simulation Conditions

At  $t = 0$  the circuit in Fig. 1 is switched on, then  $V_g$  is applied, through  $C_2$ , to the preionised discharge gap. The kinetics of electrons and ions in the discharge are simulated by repeating the calculation every time step  $\Delta t$  using an explicit method. During  $\Delta t$ , the values of  $E(z, t)$  and other parameters are assumed to be constant. After calculation of the density for the  $j$ th species, a new  $V_g$  is calculated using the numerical method of Runge–Kutta (Akashi *et al.* 1994). Then,  $E(z, t)$  is calculated using the method of successive-over-relaxation (SOR) in the cylindrical coordinates.

Here  $\Delta t$  is taken to be 1 ps. The discharge space is divided into 50 in the  $x$  direction and 25 in the  $r$  direction. The size in non-uniform space grids near the electrodes is finest, and increases exponentially from the electrodes in the

direction of the centre of the gap. In the radius direction, the grid size increases exponentially with  $r$  as shown in Fig. 2.

The total gas pressure and the ratio of the Ar/F<sub>2</sub>/He mixture are taken to be 1900 Torr (253 kPa) and 0.0789/0.0024/0.9187 respectively. The values of  $\mu$  and  $\gamma_p$  in equation (5) are estimated to be 0.041 cm<sup>-1</sup> and  $2.0 \times 10^{-2}$  respectively. The lifetime of ArF\* for spontaneous emission is taken to be 4.2 ns (Ohwa and Obara 1988). The discharge volume is assumed to be 1 cm  $\times$  90 cm<sup>2</sup> (gap distance  $d$  times the discharge cross section  $S$ ). The number density of preionised electron-ion pairs  $n_{e0}$  is taken to be  $10^6$  and  $10^8$  cm<sup>-3</sup>, and their energy is 1 eV.

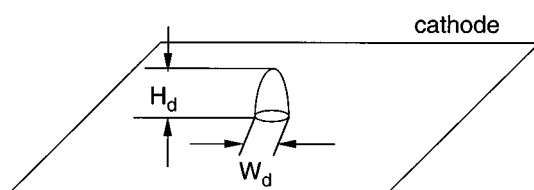


**Fig. 3.** Configuration of a sharp protrusion on the cathode. Here  $H_d$  is assumed to be 1  $\mu\text{m}$  and  $W_d$  to be 0.2  $\mu\text{m}$ .

A sharp protrusion on the cathode surface is assumed to be located at  $x = 0$  and  $r = 0$  as shown in Fig. 3, and its radius  $r_{\text{max}}$  is 0.5 cm.

### 3. Results and Discussion

#### (3a) Discharge Voltage and Current Waveforms

Fig. 4 shows the discharge voltage  $V_g$  and current  $I_g$  waveforms along with the laser output waveform for  $n_{e0} = 10^6$  and  $10^8$  cm<sup>-3</sup>. They are typical for discharge-excited excimer lasers (Green and Brau 1986; Date *et al.* 1988; Akashi *et al.* 1994). The micro-streamer appears in the time range between the decay of  $V_g$  and the onset of the laser oscillation.

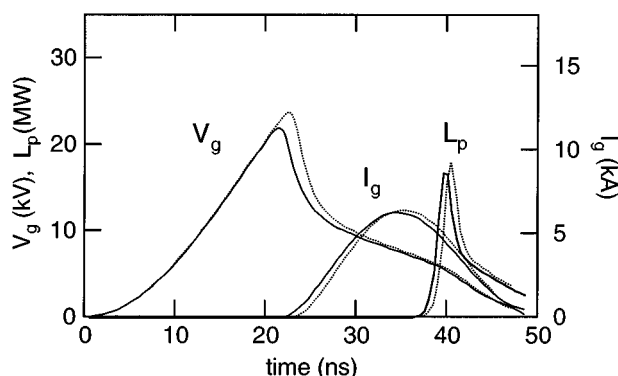


**Fig. 4.** Waveforms of the discharge voltage  $V_g$  and current  $I_g$  along with laser output for  $n_{e0} = 10^8$  cm<sup>-3</sup> (solid curves) and  $n_{e0} = 10^6$  cm<sup>-3</sup> (dotted curves).

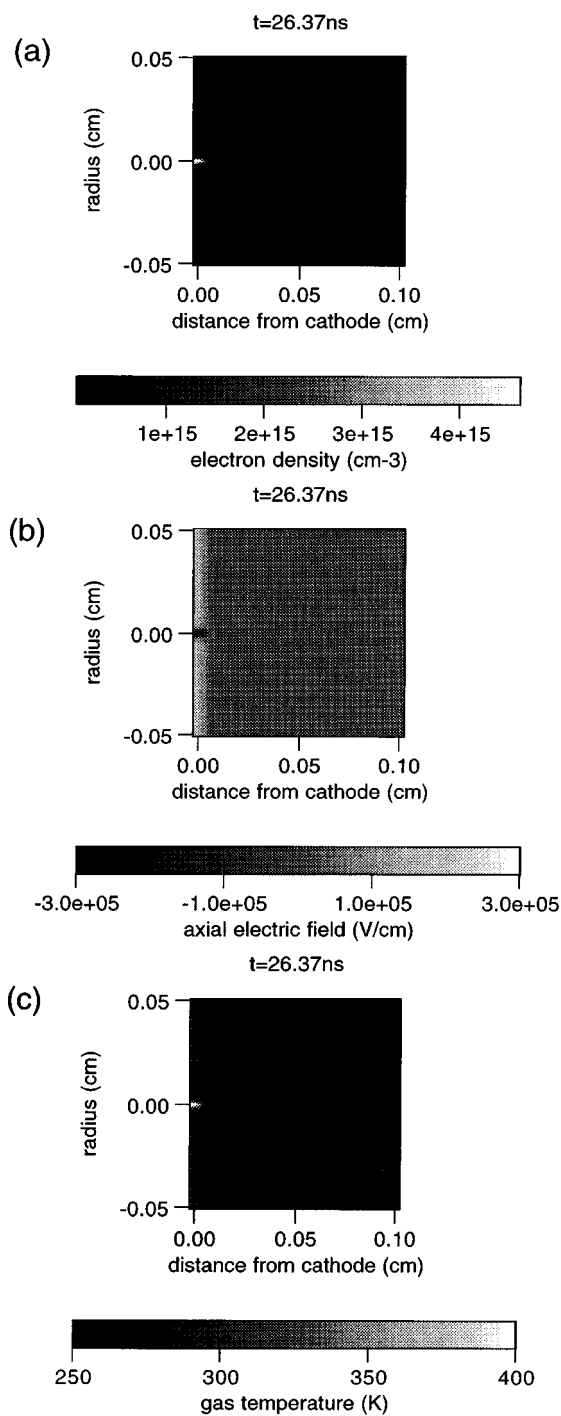


**Fig. 5.** Spatial distribution of  $n_e$ ,  $E_x$  and  $T_g$  after the first shot of discharge near the protrusion in the case of  $n_{e0} = 10^8 \text{ cm}^{-3}$ : (a) the electron density  $n_e = 1.7 \times 10^{16} \text{ cm}^{-3}$  at the protrusion; (b) the axial electric field  $E_x = -1.9 \times 10^6 \text{ V cm}^{-1}$  at the protrusion; and (c) the gas temperature  $T_g > 1000 \text{ K}$  at the protrusion.

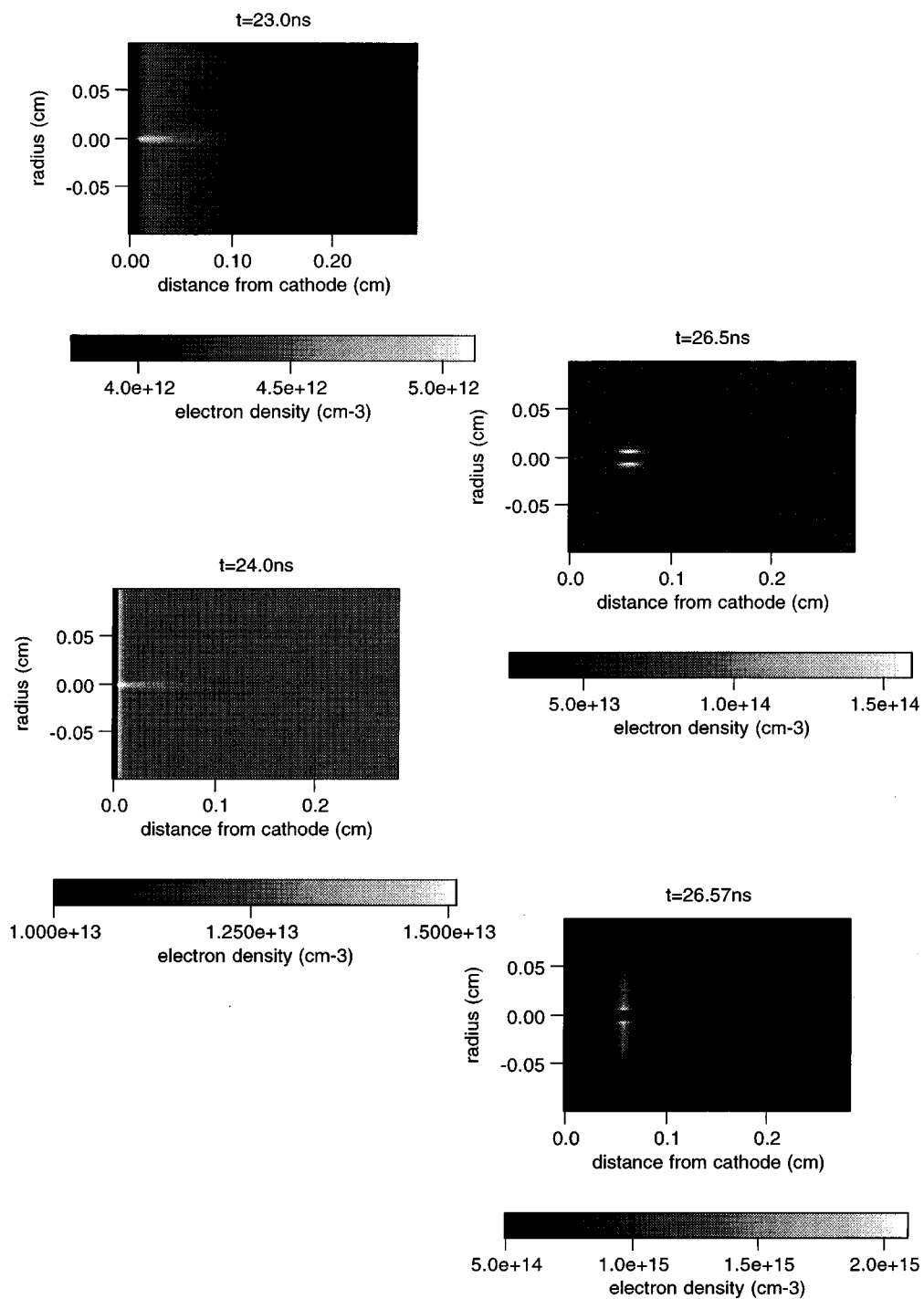


**Fig. 6a.** Spatial distribution of the electron number density  $n_e$  for various time steps for  $n_{e0}$ : (a)  $10^8 \text{ cm}^{-3}$  and (b)  $10^6 \text{ cm}^{-3}$ .

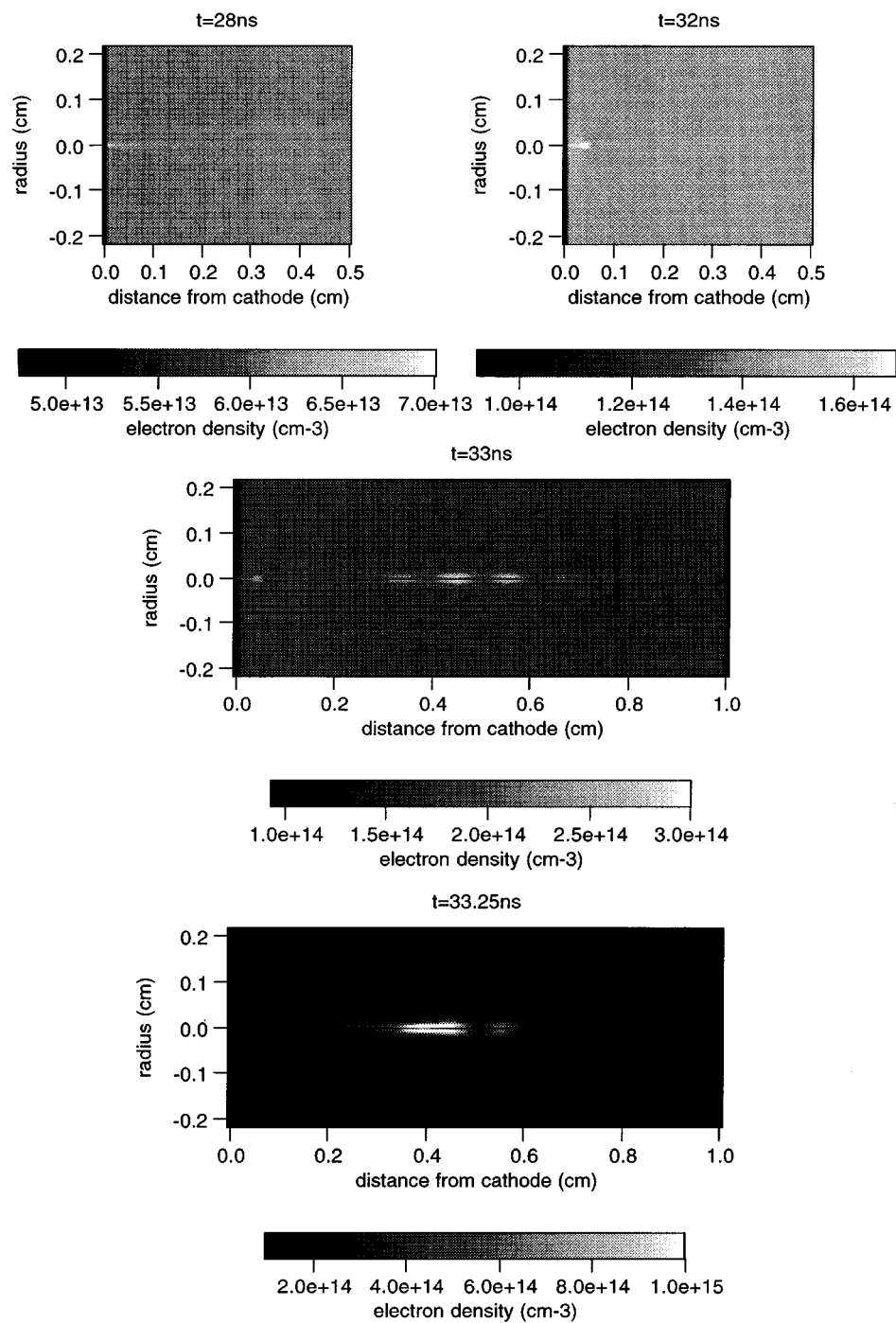


Fig. 6b

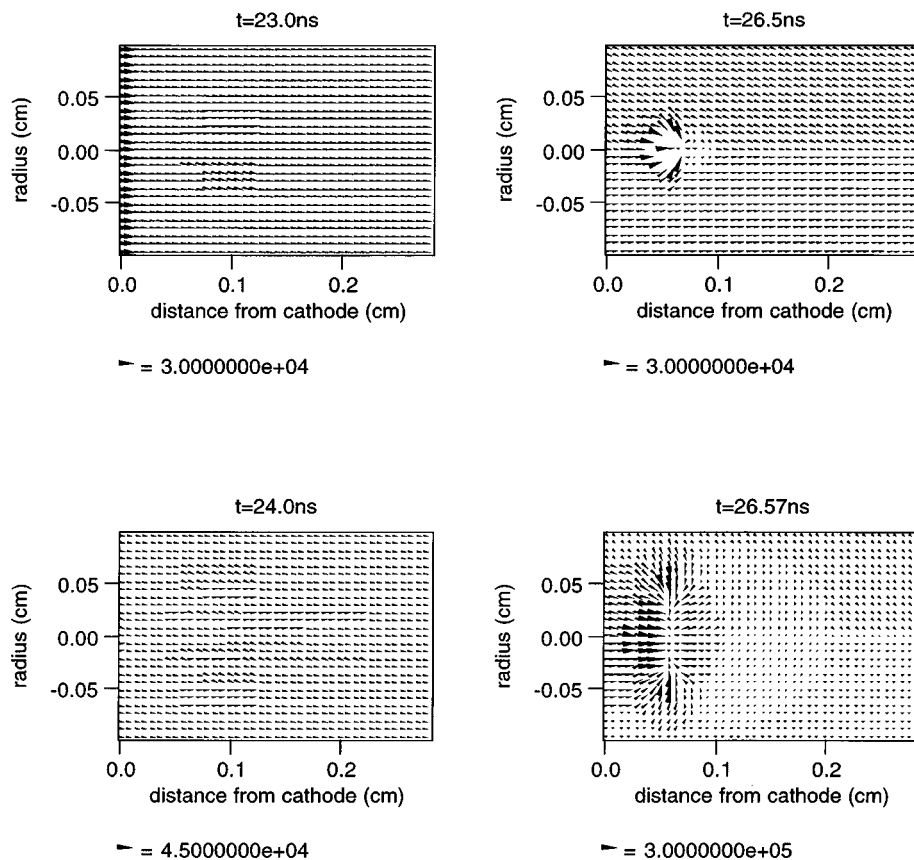


Fig. 7a. Spatial distribution of the electric field strength  $E$  for various time steps for  $n_{e0}$ : (a)  $10^8 \text{ cm}^{-3}$  and (b)  $10^6 \text{ cm}^{-3}$ .

### (3b) Initiation of Micro-streamer

The field strength at the protrusion shown in Fig. 3 is evaluated to be more than  $1\text{--}10 \text{ MV cm}^{-1}$ , because the average field in the vicinity of the cathode was  $200 \text{ kV cm}^{-1}$  according to the result of one-dimensional modeling (Akashi *et al.* 1994, 1995). The protrusions on the cathode surfaces are believed to trigger micro-discharges and trace spots on the surface (Dreiskemper and Boettcher 1995).

In the present modeling, for the first shot of discharge the initial gas temperature is assumed to be uniform over all the gap and to be 273 K. Fig. 5 shows the spatial distribution of  $n_e$ ,  $E_x$  and  $T_g$  after the first shot of discharge for  $n_{e0} = 10^6 \text{ cm}^{-3}$ . For the case of  $n_{e0} = 10^8 \text{ cm}^{-3}$ , their patterns and magnitudes are almost the same as those for  $10^6 \text{ cm}^{-3}$ . In Fig. 5a the  $n_e$  value at the protrusion is shown to be  $1.7 \times 10^{16} \text{ cm}^{-3}$  by strong field emission, while  $n_e$  in the bulk is  $10^{13} \text{ cm}^{-3}$ . Accordingly  $n_+$  at the protrusion is  $1.2 \times 10^{15} \text{ cm}^{-3}$ , while in the bulk it is  $7 \times 10^{13} \text{ cm}^{-3}$ . Fig. 5b shows that the axial component  $E_x$  at

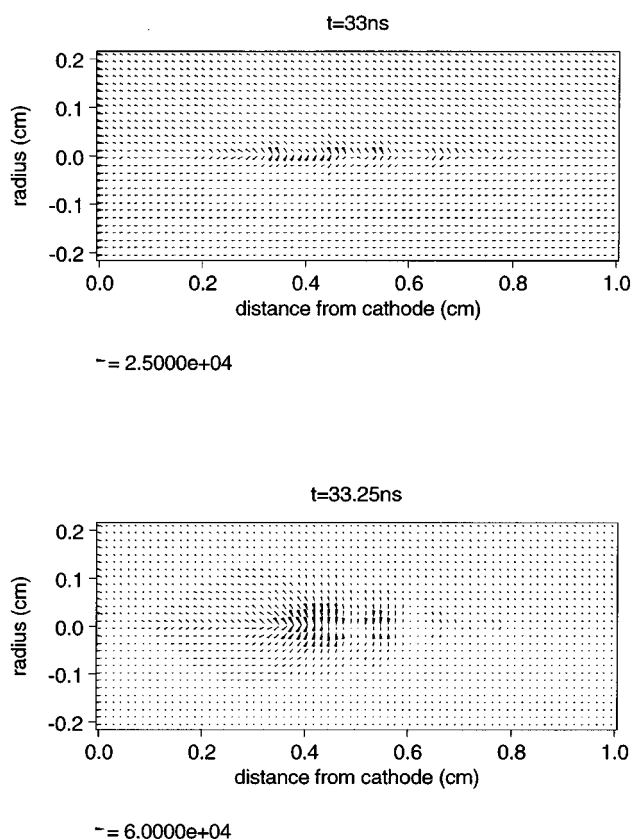


Fig. 7b

the protrusion is  $-2 \times 10^6 \text{ V cm}^{-1}$  due to strong negative space charge produced by the field emission, and  $+4 \times 10^5 \text{ V cm}^{-1}$  in the cathode area and  $+10^4 \text{ V cm}^{-1}$  in the discharge bulk. It was also seen at the protrusion that  $E_x$  oscillated between positive and negative values over time, depending on the balance of the magnitude of emission and diffusion of electrons. The  $T_g$  at the protrusion is found to be around 1000 K, while the background gas temperature is 273 K as shown in Fig. 5c. At the first shot, the discharge uniformity is broken only at the protrusion area. In the following shots, the space charge may disappear due to recombination, however the locally heated gas temperature might influence and trigger micro-streamers.

### (3c) Spatio-temporal Development of Micro-streamers

Once gas particles in the high field region, e.g. in the vicinity of the cathode, are heated, they may grow to a micro-streamer by the next shot of discharge. The following figures are the results obtained by the second shot, taking the  $T_g$  distribution shown in Fig. 5c as an initial condition.

*Evolution of Electron Number Density  $n_e$ :* Fig. 6 shows the spatial distribution of  $n_e$  for  $t = 23\text{--}33.25 \text{ ns}$ .

In the case of  $n_{e0} = 10^8 \text{ cm}^{-3}$  (Fig. 6a), the high  $n_e$  region which is several times higher than the background is seen in a filament shape and extends from the protrusion to  $\sim 1 \text{ mm}$  in the anode direction at  $t \sim 25 \text{ ns}$ . With increasing  $n_e$ , the filament shaped region starts to expand radially from  $t \sim 25 \text{ ns}$  and stops its extension in the anode direction any further. The high  $n_e$  region expands until its diameter becomes around  $1 \text{ mm}$  at  $x = 0.5 \text{ mm}$ . This phenomenon may be explained by the decay of  $V_g$  and the accumulation of negative space charge at the top of the micro-streamer. These highly concentrated electrons diffuse into the surroundings, and  $n_e$  becomes uniform spatially. It is interesting to note that in the centre of the filament the concentration is lower than that at larger  $r$ . This phenomenon is explained also in connection with the evolution of  $E$  shown in Fig. 7a.

On the other hand, in the case of  $n_{e0} = 10^6 \text{ cm}^{-3}$  in Fig. 6b, the behaviour of the micro-streamer is quite different from the former case. At the beginning of the evolution, for  $t$  less than  $32 \text{ ns}$ , the behaviour is similar to the case of  $n_{e0} = 10^8 \text{ cm}^{-3}$ . At  $t = 33 \text{ ns}$ , the micro-streamer develops significantly toward the anode and its head is about  $0.1 \text{ cm}$  from the anode. This rapid extension is due to the propagation of the field distortion and high  $V_g$  values (see Fig. 4). After  $t = 33.25 \text{ ns}$ , the cathode directed micro-streamer was obtained in detailed observations, though we cannot observe this in the present black and white figures. The radius of the streamer is about  $70 \mu\text{m}$ . These features are consistent with the observations of Dreiskemper and Boettcher (1995) and Taylor (1986) and indicate that the high preionisation may suppress evolution of filamental discharge.

*Evolution of Electric Field  $E$ :* The time and spatial evolution of  $E$  is shown in Fig. 7 using vector arrows. The size and the direction of the arrows correspond to the magnitude and the direction to which electrons are forced.

In the case of  $n_{e0} = 10^8 \text{ cm}^{-3}$  (Fig. 7a),  $E$  in the bulk is almost uniform up to  $24 \text{ ns}$ , however an appreciable enhancement at the cathode is seen. After  $t = 26 \text{ ns}$  the radial component  $E_r$  at the protrusion becomes significant. However,  $E_x$  in the bulk region stops its expansion, because  $V_g$  is decaying and negative space charge accumulates at the head of the streamer in this time span.

In the bulk region  $E$  is uniform and low since  $n_e \approx n_+$ . In the case of  $n_{e0} = 10^6 \text{ cm}^{-3}$  (Fig. 7b),  $E$  in the bulk is larger than that for  $n_{e0} = 10^8 \text{ cm}^{-3}$  case because the former  $V_g$  is larger than the latter. This high  $E$  makes the micro-streamer extend significantly.

*Evolution of Mean Electron Energy  $\bar{\epsilon}$ :* Fig. 8 shows the spatial  $\bar{\epsilon}$  distribution for  $n_{e0} = 10^6 \text{ cm}^{-3}$ . For  $t < 33 \text{ ns}$ , the  $\bar{\epsilon}$  value in the bulk region varies depending on  $x$  but almost no change in the radial direction. On the other hand  $\bar{\epsilon}$  in the cathode fall region is constant and is around  $6 \text{ eV}$ . For  $t > 33 \text{ ns}$   $\bar{\epsilon}$  becomes more than  $10 \text{ eV}$  at positions where  $T_g$  is very high (see Fig. 9). The region of high  $\bar{\epsilon}$  values is seen in the area of around  $x = 4 \text{ mm}$  and  $r = 0.5 \text{ mm}$  as a ring shape. It is seen at  $t = 33 \text{ ns}$  that  $\bar{\epsilon}$  at the head of the streamer around  $x = 0.6 \text{ cm}$  is slightly lower than the background value. The  $\bar{\epsilon}$  in the bulk region decreases with time because of the decay of  $V_g$ .

*Evolution of Gas Temperature  $T_g$ :* Fig. 9 shows the spatial distribution of  $T_g$  for  $n_{e0} = 10^6 \text{ cm}^{-3}$ . At  $t = 24 \text{ ns}$ ,  $T_g$  at the cathode is around  $10 \text{ K}$  higher than the background. At the protrusion  $T_g$  become highest and is  $568 \text{ K}$  at  $t = 32 \text{ ns}$ ,

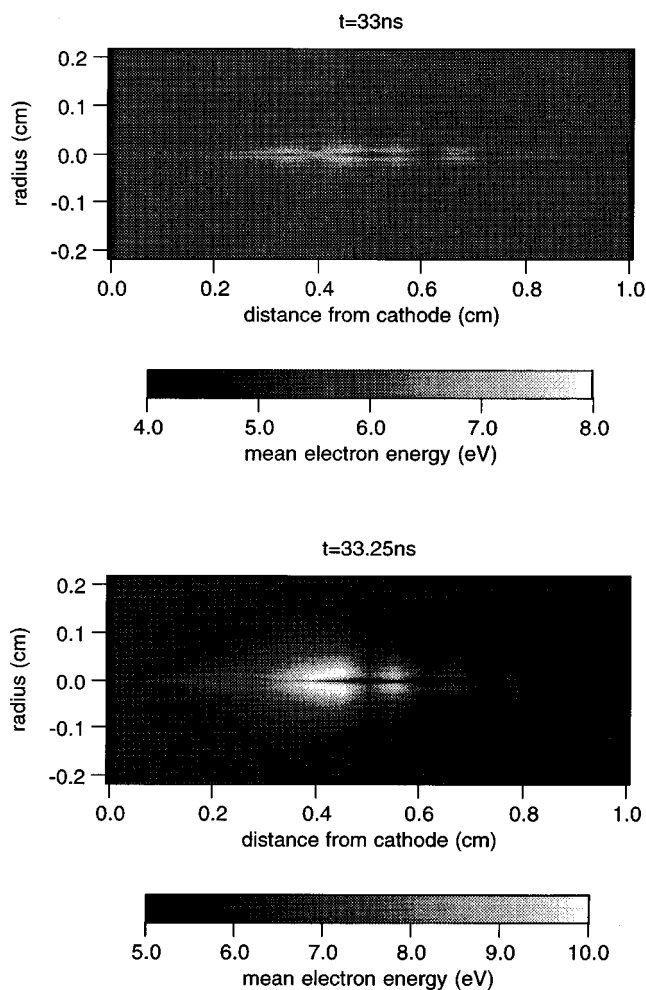
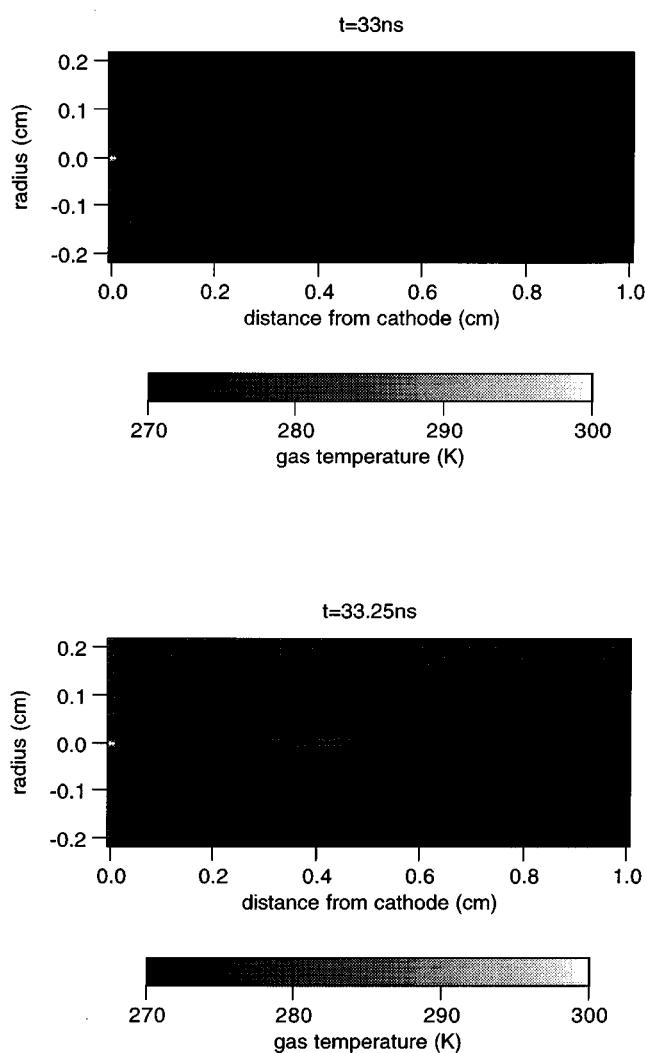


Fig. 8. Spatial distribution of the mean electron energy  $\bar{\epsilon}$  for various time steps for  $n_{e0} = 10^6 \text{ cm}^{-3}$ .

565 K at  $t = 33 \text{ ns}$  and 564 K at 33.25 ns. Note that at  $t = 33.25 \text{ ns}$  the region where  $T_g$  is higher than the background corresponds to the region where  $\bar{\epsilon}$  is higher. The  $T_g$  at the head of the streamer is only around 10 K higher than the background.

### (3d) Discussion on Initiation of a Micro-streamer

It has been reported that micro-streamers (filamentary discharges) might be initiated due to non-uniform discharge by depression of halogen donors (Kushner 1991), deficiency in the uniformity of preionised electron-ion pairs (Taylor 1986; Kushner 1991), etc. However, the negative F ion density was shown to accumulate up to around  $10^{14} \text{ cm}^{-3}$  at most by Akashi *et al.* (1994, 1995), which was about 0.06% of the initial  $\text{F}_2$  concentration. This result may not indicate that the reason of halogen donor depression leads to instability.



**Fig. 9.** Spatial distribution of the gas temperature  $T_g$  for various time steps for  $n_{e0} = 10^6 \text{ cm}^{-3}$ .

Generally, the initiation of instability has been observed by Dreiskemper and Boetticher (1995), Makarov (1995) and Makarov and Bychkov (1996). The local strong emission of electrons from the cathode, through heating up the gas, may bring filamental instability with high probability. Dreiskemper and Boetticher (1995) observed that micro-streamers sometimes accompany cathode hot-spots.

The present results for the evolution of  $n_e$ ,  $E$ ,  $\bar{\varepsilon}$  and  $T_g$  are qualitatively consistent with the observations mentioned above. As a result the present model in which micro-streamers are triggered by non-uniform  $T_g$  in the vicinity of the cathode through strong field emission of electrons may be one of the causes of instability in uniform volume discharges.

#### 4. Conclusion

A two-dimensional model for examining micro-discharge evolution in a discharge-excited ArF laser was presented. The entire processes from initiation of a micro-discharge and its development were described. The results are summarised as follows.

- (1) In the present model, a filamentary discharge appears in the vicinity of the cathode at which the local field is extremely high.
- (2) The gas temperature in the micro-streamer is higher than that in the volume discharge region and is around 500 K. The temperature at the protrusion on the cathode is around 1000 K.
- (3) The micro-streamer is extended significantly in the anode direction when the preionised electron density is low. This result indicates the fact that the high concentration of preionisation controls the discharge instability.

#### Acknowledgment

The authors would like to thank Professor T. Sasaki and Dr N. Takahashi at the National Defense Academy for supporting this work and for helpful discussions.

#### References

- Akashi, H., Sakai, Y., and Tagashira, H. (1994). *J. Phys. D* **27**, 1097–1106.
- Akashi, H., Sakai, Y., and Tagashira, H. (1995). *J. Phys. D* **28**, 445–51.
- Date, H., Kakizaki, K., Sakai, Y., and Tagashira, H. (1988). Ninth Int. Conf. on Gas Discharges and Their Application, Venice, pp. 705–8.
- Dreiskemper, R., and Boettcher, W. (1995). *IEEE Trans. Plasma Science* **23**, 987–95.
- Graves, D. B., and Jensen, K. F. (1986). *IEEE Trans. Plasma Sci.* **PS-14**, 78–91.
- Green, A. E., and Brau, C. A. (1978). *IEEE J. Quant. Electron.* **QE-14**, 951–7.
- Kushner, M. J. (1991). *IEEE Trans. Plasma Sci.* **PS-19**, 387–99.
- Makarov, M. (1995). *J. Phys. D* **28**, 1083–93.
- Makarov, M., and Bychkov, Y. (1996). *J. Phys. D* **29**, 350–63.
- Morrow, R. (1985). *Phys. Rev. A* **32**, 1799–1809.
- Ohwa, M., and Obara, M. (1988). *J. Appl. Phys.* **63**, 1306–12.
- Taylor, R. S. (1986). *Appl. Phys. B* **41**, 1–24.

*Manuscript received 17 July 1996, accepted 17 January 1997*